Journal of Intelligent Material Systems and Structures

Original Article

Journal of Intelligent Material Systems and Structures
2018, Vol. 29(19) 3696–3709

DOI: 10.1177/1045389X18798954
journals.sagepub.com/home/jim
SAGE

# Phenomenological modeling of the thermo-magneto-mechanical behavior of magnetic shape memory alloys

**Vandré F de Souza[1], Marcelo A Savi[1], Luciana L Silva Monteiro[2] and Alberto Paiva[3]**

**Abstract**

Magnetic shape memory alloy is an interesting class of material that offers fast and contactless actuation associated with large deformation. This article deals with a novel constitutive model based on internal variables that describes the phenomenological behavior of magnetic shape memory alloys. Model formulation is developed within the framework of continuum mechanics and thermodynamics defining a mixture free energy potential based on four macroscopic phases. Zeeman effect is considered to incorporate the magnetic behavior. A numerical procedure is proposed to deal with the model nonlinearities. Model predictions are presented for different thermo-magneto-mechanical loadings treating reorientation and phase transformations. Numerical simulations are carried out showing the model capabilities and comparisons with experimental data available in the literature attesting its ability to capture the general thermo-magneto-mechanical behavior of magnetic shape memory alloys.

**Keywords**

Magnetic shape memory alloys, constitutive modeling, actuators, magnetic field–induced phase transformation, magnetic field–induced reorientation

## Introduction

The so-called smart materials have an increasing importance on the design of new adaptive mechanical systems built with sensors and actuators. This adaptive behavior allows one to alter shape and physical properties by imposing electric or magnetic fields, as well as changing its temperature or stress. In this regard, magnetic shape memory alloys (MSMAs) have emerged as an interesting alternative of this class of materials presenting the ability to convert magnetic energy into mechanical energy. The first research related to MSMAs dated to 1996 when $Ni_2MnGa$ single crystals presented a strain of 0.2% under a moderate field of 1 T (Ullakko et al., 1996). These alloys exhibit an interesting coupling between elastic and magnetic properties that can be observed by applying a magnetic field.

Two mechanisms can explain the magnetic field–induced strain (MFIS): the reorientation of martensitic variants (Karaca et al., 2007, 2003) and field-induced phase transformation (Kainuma et al., 2006; Karaca et al., 2007, 2009). The MFIS has the same order as the highest magnetostriction obtained in magnetostrictive materials such as $Tb_{0.27}Dy_{0.73}$ and Terfenol-D (Ullakko et al., 1996). Materials such as Ni-Mn-Ga started presenting strain levels of 6%–10% using the variant reorientation mechanism (Marioni et al., 2005; Murray et al., 2000; Tickle and James, 1999) introducing new perspectives of the production of power and motion, combining advantages of traditional SMA characteristics with large frequencies to 1–2 kHz (Henry et al., 2002) in the presence of moderate magnetic fields.

Field-induced martensitic variant reorientation is considered as the main mechanism for MFIS. The NiGaMn and NiCoMnIn usually need large magnetic fields to complete the transformation from martensite to austenite using magnetic field–induced transformations (Liu et al.,

[1]Center for Nonlinear Mechanics, COPPE—Department of Mechanical Engineering, Universidade Federal do Rio de Janeiro, Rio de Janeiro, Brazil
[2]Department of Mechanical Engineering, Centro Federal de Educação Tecnológica Celso Suckow da Fonseca (CEFET/RJ), Rio de Janeiro, Brazil
[3]Department of Mechanical Engineering, Volta Redonda School of Engineering, Universidade Federal Fluminense, Volta Redonda, Brazil

**Corresponding author:**
Marcelo A Savi, Center for Nonlinear Mechanics, COPPE—Department of Mechanical Engineering, Universidade Federal do Rio de Janeiro, P.O. Box 68.503, Rio de Janeiro 21941-972, Brazil.
Email: savi@mecanica.ufrj.br

2012). Nevertheless, new perspectives of applicability were shown by Bruno et al. (2017) that achieved a complete reversible transformation from martensite to austenite transformation with low values of magnetic field (1.3 T) in $Ni_{45}Co_5Mn_{36}.6In_{13.4}$ single-crystal samples using a magneto-mechanical loading process called stress-field ramping.

Several research efforts are focused on the description of the MFIS of NiMnGa and other MSMA materials. Micromagnetic models that are focused on the fundamental mechanisms in microscopic scale have been developed as an alternative to deal with MSMA description (Chernenko, 2004; James and Wuttig, 1998; Müllner et al., 2002). Phase-field models established different order parameters providing descriptions of the evolution of magnetic domains and martensitic microstructures (Jin, 2009; Li et al., 2011; Penga et al., 2017).

Phenomenological models based on thermodynamical principles constitute another alternative to describe MSMA behavior. The thermo-magneto-mechanical behavior of MSMAs has been modeled by Hirsinger and Lexcellent (2003) using this approach. The influence of the microstructure is treated using two internal variables and their evolution laws were proposed to describe variant reorientation process. In this regard, it is important to highlight the phenomenological model proposed (Kiefer et al., 2007; Kiefer and Lagoudas, 2005, 2008, 2009) that describes magnetic-induced martensitic variant reorientation process under constant mechanical load in MSMA. This model captures the general MSMA behavior presenting good correlation with experimental data.

Couch et al. (2007) developed a quasi-static model for MSMA inspired on SMA constitutive models (Brinson, 1993; Tanaka, 1986). The model captures both the MSMA and pseudoelastic behavior of the NiMnGa. The model presented an overprediction of stress at higher applied fields due to linear assumption but can capture the reorientation mechanisms of NiMnGa. Guo et al. (2014) developed a model to describe variant reorientations on MSMA using only martensitic phase. A hyperbolic tangent expression is developed to describe the variant reorientations during magnetic and mechanical loading processes.

Haldar et al. (2014) presented a thermodynamic-based phenomenological model of field-induced phase transformation for a single-crystal NiMnCoIn material. Numerical results of magneto-mechanical, magneto-thermal, and magnetization field were compared with experiments showing the model capability to describe thermo-magneto-mechanical responses.

According to Liang et al. (2003), the development of mechanical devices with MSMAs is directly related to accurate models that are usually complex due to their strong nonlinearities. Therefore, the exploration of the full engineering potential of MSMAs needs comprehensive models that allow one to reliably predict the material behavior. Motivated by this, this article deals with a novel constitutive model based on internal variables that describe the general thermo-magneto-mechanical characteristics of the MSMA phenomenological behavior. The theory is inspired on an SMA model proposed by Paiva et al. (2005) and Oliveira et al. (2016) allowing the description of the thermo-magneto-mechanical behavior of MSMA in a flexible way. Numerical simulations are carried out establishing a comparison with experimental data available in the literature.

## Constitutive theory

This article presents a novel constitutive model for MSMAs based on the model developed for classical SMAs proposed by Paiva et al. (2005) and Oliveira et al. (2016). Basically, it considers four macroscopic phases representing the austenitic phase and three variants of martensite, presenting internal constraints to define phase transformations. Here, a new thermo-magneto-mechanical version of this model is proposed, where a magnetic term is introduced allowing one to describe phase transformations induced by stress, temperature, and magnetic field, presenting a proper macroscopic description of MSMAs.

Model formulation is developed within the framework of continuum mechanics and thermodynamics considering generalized standard materials approach. In essence, the constitutive equation formulation follows mechanical principles and needs to satisfy the Clausius–Duhem inequality to be admissible (Lemaitre and Chaboche, 1990). The main idea is to propose a Helmholtz free energy ($\psi$) and a potential of dissipation ($\phi$) from which thermodynamic forces and flux equations are obtained.

Based on that, a Helmholtz free energy potential is adopted for each one of the four macroscopic phases: tensile detwinned martensite ($\mathcal{M}^+$), compressive detwinned martensite ($\mathcal{M}^-$), austenite ($\mathcal{A}$), and twinned martensite ($\mathcal{M}$). Moreover, the following state variables are considered: elastic strain, $\varepsilon^e$; temperature, $T$; and austenitic and martensitic magnetizations, $M^{\mathcal{A}}$ and $M^{\mathcal{M}}$, respectively

$$\mathcal{M}^+ : \rho\psi^+(\varepsilon^e, T) = \frac{1}{2}E^{\mathcal{M}}\varepsilon^{e2} - \alpha\varepsilon^e - \Lambda^{\mathcal{M}} - \Omega^{\mathcal{M}} (T - T_0)\varepsilon^e \tag{1}$$

$$\mathcal{M}^- : \rho\psi^-(\varepsilon^e, T) = \frac{1}{2}E^{\mathcal{M}}\varepsilon^{e2} + \alpha\varepsilon^e - \Lambda^{\mathcal{M}} - \Omega^{\mathcal{M}} (T - T_0)\varepsilon^e \tag{2}$$

$$\mathcal{A} : \rho\psi^{\mathcal{A}}\left(\varepsilon^e, T, M^{\mathcal{A}}\right) = \frac{1}{2}E^{\mathcal{A}}\varepsilon^{e2} - \Lambda^{\mathcal{A}} - \Omega^{\mathcal{A}}(T - T_0) \varepsilon^e - \mu_0 H M^{\mathcal{A}} \tag{3}$$

$$\mathcal{M}: \rho\psi^{\mathcal{M}}\left(\varepsilon^e, T, M^{\mathcal{M}}\right) = \frac{1}{2}E^{\mathcal{M}}\varepsilon^{e2} + \Lambda^{\mathcal{M}} - \Omega^{\mathcal{M}} (T - T_0)\varepsilon^e - \mu_0 H M^{\mathcal{M}} \tag{4}$$

In the previous equations, superscript $\mathcal{M}$ is related to martensitic phase, while $\mathcal{A}$ is associated with austenite. Hence, it is possible to define the following parameters: $\alpha$ is related to the stress–strain hysteresis loop height observed during the martensitic transformation, $E$ represents the elastic modulus, $\Omega$ is related to the thermal expansion coefficient, $\Lambda = \Lambda(T)$ represents temperature functions related to the phase transformation, $T_0$ is a reference temperature where the material is in a stress-free condition and therefore has no deformation, $\rho$ is the density, and $\mu_0$ is the magnetic permeability of vacuum.

A Helmholtz free energy of the four macroscopic phases' mixture is proposed by defining a volume fraction for each phase: $\beta^+$ that is associated with tensile detwinned martensite ($\mathcal{M}^+$), $\beta^-$ that is related to compressive detwinned martensite ($\mathcal{M}^-$), $\beta^{\mathcal{A}}$ that represents austenite ($\mathcal{A}$), and $\beta^{\mathcal{M}}$ that corresponds to twinned martensite ($\mathcal{M}$). Hence, the mixture free energy can be written as follows

$$\begin{aligned}&\rho\tilde{\psi}\left(\varepsilon^e, T, M^{\mathcal{A}}, M^{\mathcal{M}}, \beta^+, \beta^-, \beta^{\mathcal{A}}, \beta^{\mathcal{M}}\right)\\ &= \rho\left(\beta^+\psi^+ + \beta^-\psi^- + \beta^{\mathcal{A}}\psi^{\mathcal{A}} + \beta^{\mathcal{M}}\psi^{\mathcal{M}}\right)\\ &\quad + J_\Theta\left(\beta^+, \beta^-, \beta^{\mathcal{A}}, \beta^{\mathcal{M}}\right)\end{aligned} \tag{5}$$

where $J_\Theta(\beta^+, \beta^-, \beta^{\mathcal{A}}, \beta^{\mathcal{M}})$ represents an indicator function related to the coexistence of the four distinct phases, which is represented by constraints expressed on the following convex set

$$\begin{aligned}\Theta = \{&\beta^m \in \Re | 0 \le \beta^m \le 1 (m = +, -, \mathcal{A}, \mathcal{M});\\ &\beta^+ + \beta^- + \beta^{\mathcal{A}} + \beta^{\mathcal{M}} = 1\}\end{aligned} \tag{6}$$

According to these restrictions, it is possible to express an internal variable as function of the other three, $\beta^{\mathcal{M}} = 1 - \beta^+ - \beta^- - \beta^{\mathcal{A}}$, making possible to write the total free energy as a function of only three internal variables $(\beta^+, \beta^-, \beta^{\mathcal{A}})$

$$\begin{aligned}&\rho\psi\left(\varepsilon^e, T, M^{\mathcal{A}}, M^{\mathcal{M}}, \beta^+, \beta^-, \beta^{\mathcal{A}}\right)\\ &= \left\{\beta^+\left[-\alpha\varepsilon^e - \Lambda + \mu_0 H M^{\mathcal{M}}\right] + \beta^-\left[\alpha\varepsilon^e - \Lambda + \mu_0 H M^{\mathcal{M}}\right]\right.\\ &+ \beta^{\mathcal{A}}\left[\frac{1}{2}(E^{\mathcal{A}} - E^{\mathcal{M}})\varepsilon^{e^2} - \Lambda^{\aleph} - (\Omega^{\mathcal{A}} - \Omega^{\mathcal{M}})\right.\\ &\quad \left.(T - T_0)\varepsilon^e - \mu_0 H(M^{\mathcal{A}} - M^{\mathcal{M}})\right]\\ &\left.+\frac{1}{2}E^{\mathcal{M}}\varepsilon^{e2} + \Lambda^{\mathcal{M}} - \Omega^{\mathcal{M}}(T - T_0)\varepsilon^e + \mu_0 H M^{\mathcal{M}}\right\}\\ &+ J_\pi\left(\beta^+, \beta^-, \beta^{\mathcal{A}}\right)\end{aligned} \tag{7}$$

where $J_\pi = J_\pi(\beta^+, \beta^-, \beta^{\mathcal{A}})$ is the new indicator function of the convex set $\pi$, which establishes the constraints associated with the phases' coexistence defined as follows

$$\begin{aligned}\pi = \{&\beta^m \in \Re | 0 \le \beta^m \le 1 (m = +, -, \mathcal{A});\\ &\beta^+ + \beta^- + \beta^{\mathcal{A}} \le 1\}\end{aligned} \tag{8}$$

Functions $\Lambda = \Lambda(T)$ and $\Lambda^{\aleph} = \Lambda^{\aleph}(T)$ are temperature-dependent parameters responsible to define the critical transformation stress, given by

$$\Lambda = 2\Lambda^{\mathcal{M}} = \begin{cases} -L_0 + \frac{L}{T^{\mathcal{M}}}\left(T - T^{\mathcal{M}}\right) & \text{if } T > T^{\mathcal{M}} \\ -L_0 & \text{if } T \le T^{\mathcal{M}} \end{cases} \tag{9}$$

$$\Lambda^{\aleph} = \Lambda^{\mathcal{M}} + \Lambda^{\mathcal{A}} = \begin{cases} -L_0^{\mathcal{A}} + \frac{L^{\mathcal{A}}}{T^{\mathcal{M}}}\left(T - T^{\mathcal{M}}\right) & \text{if } T > T^{\mathcal{M}} \\ -L_0^{\mathcal{A}} & \text{if } T \le T^{\mathcal{M}} \end{cases} \tag{10}$$

where $T^{\mathcal{M}}$ is the temperature below which the martensitic phase is stable in a stress-free state. Moreover, $L_0, L, L_0^{\mathcal{A}}$, and $L^{\mathcal{A}}$ are parameters related to phase transformation critical stress. An additive decomposition is assumed in such a way that the elastic strain may be written as follows

$$\varepsilon^e = \varepsilon + \alpha^h\left(\beta^- - \beta^+\right) \tag{11}$$

where $\alpha^h$ is a parameter associated with the stress–strain hysteresis loop width. By replacing equation (11) in equation (7), the final form of the mixture total free energy function is obtained

$$\begin{aligned}&\rho\psi\left(\varepsilon^e, T, M^{\mathcal{A}}, M^{\mathcal{M}}, \beta^+, \beta^-, \beta^{\mathcal{A}}\right)\\ &= \left\{\beta^+\left[-\alpha\left(\varepsilon + \alpha^h(\beta^- - \beta^+)\right) - \Lambda + \mu_0 H M^{\mathcal{M}}\right]\right.\\ &+ \beta^-\left[\alpha\left(\varepsilon + \alpha^h(\beta^- - \beta^+)\right) - \Lambda + \mu_0 H M^{\mathcal{M}}\right]\\ &+ \beta^{\mathcal{A}}\left[\frac{1}{2}\left(E^{\mathcal{A}} - E^{\mathcal{M}}\right)\left(\varepsilon + \alpha^h(\beta^- - \beta^+)\right)^2 - \Lambda^{\aleph}\right.\\ &- (\Omega^{\mathcal{A}} - \Omega^{\mathcal{M}})(T - T_0)(\varepsilon + \alpha^h(\beta^- - \beta^+))\\ &\quad \left.- \mu_0 H(M^{\mathcal{A}} - M^{\mathcal{M}})\right]\\ &+ \frac{1}{2}E^{\mathcal{M}}\left(\varepsilon + \alpha^h(\beta^- - \beta^+)\right)^2 + \Lambda_{\mathcal{M}}\\ &\quad \left.- \Omega^{\mathcal{M}}(T - T_0)\left(\varepsilon + \alpha^h(\beta^- - \beta^+)\right) - \mu_0 H M^{\mathcal{M}}\right\}\\ &+ J_\pi\left(\beta^+, \beta^-, \beta^{\mathcal{A}}\right)\end{aligned} \tag{12}$$

Under this assumption and according to the formalism of standard generalized materials (Lemaitre and Chaboche, 1990), thermodynamic forces are defined as follows

$$\sigma = \rho\frac{\partial\psi}{\partial\varepsilon} = E\left(\varepsilon + \alpha^h\left(\beta^- - \beta^+\right)\right) + \alpha\left(\beta^- - \beta^+\right) - \Omega(T - T_0) \tag{13}$$

$$F^+ = -\rho\frac{\partial\psi}{\partial\beta^+} = \alpha\varepsilon + \Lambda + \beta^-\left(2\alpha^h\alpha + E\alpha^{h2}\right) - \beta^+\left(2\alpha^h\alpha + E\alpha^{h2}\right) + \alpha^h[E\varepsilon - \Omega(T - T_0)] - \mu_0 H M^{\mathcal{M}} - \lambda_\pi^+ \tag{14}$$

$$F^- = -\rho\frac{\partial\psi}{\partial\beta^-} = -\alpha\varepsilon + \Lambda + \beta^+\left(2\alpha^h\alpha + E\alpha^{h2}\right) - \beta^-\left(2\alpha^h\alpha + E\alpha^{h2}\right) - \alpha^h[E\varepsilon - \Omega(T - T_0)] - \mu_0 H M^{\mathcal{M}} - \lambda_\pi^- \tag{15}$$

$$F^{\mathcal{A}} = -\rho\frac{\partial\psi}{\partial\beta^{\mathcal{A}}} = -\frac{1}{2}\left(E^{\mathcal{A}} - E^{\mathcal{M}}\right)\left(\varepsilon + \alpha^h\left(\beta^- - \beta^+\right)\right)^2 + \Lambda^{\aleph} + \left(\Omega^{\mathcal{A}} - \Omega^{\mathcal{M}}\right)(T - T_0)\left(\varepsilon + \alpha^h\left(\beta^- - \beta^+\right)\right) + \mu_0 H\left(M^{\mathcal{A}} - M^{\mathcal{M}}\right) - \lambda_\pi^{\mathcal{A}} \tag{16}$$

$$F^{M^{\mathcal{A}}} = \frac{\rho}{\mu_0}\left(\frac{\partial\psi}{\partial M^{\mathcal{A}}}\right) = -H\beta^{\mathcal{A}} \tag{17}$$

$$F^{M^{\mathcal{M}}} = \frac{\rho}{\mu_0}\left(\frac{\partial\psi}{\partial M^{\mathcal{M}}}\right) = H\left(\beta^+ + \beta^- + \beta^{\mathcal{A}} - 1\right) \tag{18}$$

where $\sigma$ represents the stress, and $\lambda_\pi = (\lambda_\pi^+, \lambda_\pi^-, \lambda_\pi^{\mathcal{A}})$ is a Lagrange multiplier set defined from the projections to the convex set $\pi$. This is equivalent to the subdifferentials of the indicator function $J_\pi$ with respect to volume fractions (Paiva et al., 2005; Rockafellar, 1970). Furthermore, parameters $E$ and $\Omega$ can be defined from their correspondent values for austenitic and martensitic phases, as follows

$$E = E^{\mathcal{M}} + \beta^{\mathcal{A}}\left(E^{\mathcal{A}} - E^{\mathcal{M}}\right) \tag{19}$$

$$\Omega = \Omega^{\mathcal{M}} + \beta^{\mathcal{A}}\left(\Omega^{\mathcal{A}} - \Omega^{\mathcal{M}}\right) \tag{20}$$

Besides, it is possible to define the magnetization, $\mathbb{M}$, given by

$$\mathbb{M} = \mu_0\left(M^{\mathcal{M}}\beta^{\mathcal{M}} + M^{\mathcal{A}}\beta^{\mathcal{A}}\right) \tag{21}$$

## Dissipation processes

Since MSMAs have a nonlinear dissipative behavior, the free energy potential ($\psi$) is not sufficient for obtaining the constitutive equations. Therefore, it is necessary to introduce a potential of dissipation, or its dual, $\phi^*$, in order to describe the evolution of irreversible processes. The following definition is adopted to describe MSMA behavior

$$\phi^* = \frac{1}{2\eta^{\mathcal{M}}}\left(F^+\right)^2 + \frac{1}{2\eta^{\mathcal{M}}}\left(F^-\right)^2 + \frac{1}{2\eta^{\mathcal{A}}}\left(F^{\mathcal{A}}\right)^2 + \tilde{g}\left(H, F^{M^{\mathcal{M}}}\right) + \tilde{h}\left(H, F^{M^{\mathcal{A}}}\right) \tag{22}$$

Following the standard generalized material approach, it is possible to obtain the evolution equations

$$\dot{\beta}^+ \in \partial_{F^+}\phi^* = \frac{F^+}{\eta^{\mathcal{M}}} \tag{23}$$

$$\dot{\beta}^- \in \partial_{F^-}\phi^* = \frac{F^-}{\eta^{\mathcal{M}}} \tag{24}$$

$$\dot{\beta}^{\mathcal{A}} \in \partial_{F^{\mathcal{A}}}\phi^* = \frac{F^{\mathcal{A}}}{\eta^{\mathcal{A}}} \tag{25}$$

$$\dot{M}^{\mathcal{M}} \in \partial_{F^{M^{\mathcal{M}}}}\phi^* = g(H) \tag{26}$$

$$\dot{M}^{\mathcal{A}} \in \partial_{F^{M^{\mathcal{A}}}}\phi^* = h(H) \tag{27}$$

Note that $g(H)$ and $h(H)$ describe the evolution of martensitic and austenitic magnetizations, being functions of the magnetic field, which means that the temperature dependence is neglected.

## Constitutive equations

A complete set of constitutive equations can be obtained from the thermodynamic forces and flux equations. Basically, the stress is a sum of reversible and irreversible parts and the thermodynamic forces (equations (14) to (18)) need to be combined with (equations (23) to (27)). Since the potential of dissipation is convex, positive, and vanishes at the origin, the Clausius–Duhem inequality is automatically satisfied under the condition that the entropy is defined as $s = -\partial\psi/\partial T$. Hence, the following set of equations is employed to describe the MSMA thermo-magneto-mechanical behavior

$$\sigma = E\left(\varepsilon + \alpha^h\left(\beta^- - \beta^+\right)\right) + \alpha\left(\beta^- - \beta^+\right) - \Omega(T - T_0) \tag{28}$$

$$\dot{\beta}^+ = \frac{1}{\eta^{\mathcal{M}}}\{\alpha\varepsilon + \Lambda + \beta^-(2\alpha^h\alpha + E\alpha^{h2}) - \beta^+\left(2\alpha^h\alpha + E\alpha^{h2}\right) + \alpha^h[E\varepsilon - \Omega(T - T_0)] - \mu_0 H M^{\mathcal{M}} - \lambda_\pi^+\} \tag{29}$$

$$\dot{\beta}^- = \frac{1}{\eta^{\mathcal{M}}}\{-\alpha\varepsilon + \Lambda + \beta^+(2\alpha^h\alpha + E\alpha^h 2) - \beta^-(2\alpha^h\alpha + E\alpha^h 2) - \alpha^h[E\varepsilon - \Omega(T - T_0)] - \mu_0 H M^{\mathcal{M}} - \lambda_\pi^-\} \tag{30}$$

$$\dot{\beta}^{\mathcal{A}} = \frac{1}{\eta^{\mathcal{A}}}\left\{ -\frac{1}{2}(E^{\mathcal{A}} - E^{\mathcal{M}})(\varepsilon + \alpha^{h}(\beta^{-} - \beta^{+}))^{2} + \Lambda^{\aleph} + (\Omega^{\mathcal{A}} - \Omega^{\mathcal{M}})(T - T_0)(\varepsilon + \alpha^{h}(\beta^{-} - \beta^{+})) + \mu_0 H(M^{\mathcal{A}} - M^{\mathcal{M}}) - \lambda_{\pi}^{\mathcal{A}} \right\} \quad (31)$$

$$\dot{M}^{\mathcal{M}} = g(H) \quad (32)$$

$$\dot{M}^{\mathcal{A}} = h(H) \quad (33)$$

In order to describe the irreversible magnetization process, the following expressions are adopted to describe martensitic and austenitic magnetization:

- Forward reorientation process ($\dot{H}>0$)

$$g = \begin{matrix} \chi^{\mathcal{M}} & \text{if } H < H_{for}^{s}(\sigma) \\ \delta^{\mathcal{M}} H & \text{if } H_{for}^{s}(\sigma) \le H \le H_{for}^{f}(\sigma) \\ 0 & \text{if } H_{for}^{f}(\sigma) < H \end{matrix} \quad (34)$$

$$h = \begin{cases} \chi^{\mathcal{A}} & \text{if } H < H_{for}^{s}(\sigma) \\ \delta^{\mathcal{A}} H & \text{if } H_{for}^{s}(\sigma) \le H \le H_{for}^{f}(\sigma) \\ 0 & \text{if } H_{for}^{f}(\sigma) < H \end{cases} \quad (35)$$

- Reverse reorientation process ($\dot{H}<0$)

$$g = \begin{cases} 0 & \text{if } H > H_{rev}^{s}(\sigma) \\ -\gamma^{\mathcal{M}} & \text{if } H_{rev}^{f}(\sigma) \le H \le H_{rev}^{s}(\sigma) \\ 0 & \text{if } H_{rev}^{f}(\sigma) > H \end{cases} \quad (36)$$

$$h = \begin{cases} 0 & \text{if } H > H_{rev}^{s}(\sigma) \\ -\gamma^{\mathcal{A}} & \text{if } H_{rev}^{f}(\sigma) \le H \le H_{rev}^{s}(\sigma) \\ 0 & \text{if } H_{rev}^{f}(\sigma) > H \end{cases} \quad (37)$$

The definitions of $g$ and $h$ are done in terms of critical magnetic field values for the activation of phase transformation and reorientation processes, inspired by Kiefer and Lagoudas (2005). Basically, four critical magnetic field values are assumed: $H_{for}^{s}, H_{for}^{f}$, $H_{rev}^{s}$, and $H_{rev}^{f}$, denoting start and finish of the forward and reverse magnetic field–induced process, respectively. These magnetic activation fields are dependent on the applied load, as shown in Figure 1 (Kiefer and Lagoudas, 2005). Based on that, these functions are expressed as follows, with parameters listed in Table 1

$$H_{rev}^{f}(\sigma) = H_{rev}^{f}(0) + a_1 \exp\left\{ -\left[\frac{(\sigma - b_1)}{2c_1}\right]^{2} \right\} \quad (38)$$

$$H_{for}^{s}(\sigma) = H_{for}^{s}(0) + a_2 \exp\left\{ -\left[\frac{(\sigma - b_2)}{2c_2}\right]^{2} \right\} \quad (39)$$

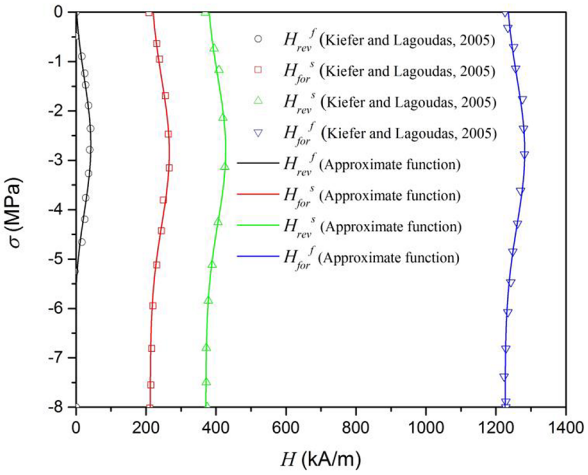


**Figure 1.** Phase diagram reported by Kiefer and Lagoudas (2005) and the proposed function to describe the activation magnetic fields in function of compressive stress.

**Table 1.** Parameters employed for proposed functions of the activation magnetic fields.

| $H_{rev}^{f}(0)$ (kA/m) | $a_1$ (kA/m) | $b_1$ (MPa) | $c_1$ (MPa) |
|---|---|---|---|
| −4.605 | 46.722 | −2.695 | 1.347 |
| $H_{for}^{s}(0)$ (kA/m) | $a_2$ (kA/m) | $b_2$ (MPa) | $c_2$ (MPa) |
| 211.981 | 54.407 | −2.834 | 1.465 |
| $H_{rev}^{s}(0)$ (kA/m) | $a_3$ (kA/m) | $b_3$ (MPa) | $c_3$ (MPa) |
| 371.263 | 56.339 | −2.795 | 1.473 |
| $H_{for}^{f}(0)$ (kA/m) | $a_4$ (kA/m) | $b_4$ (MPa) | $c_4$ (MPa) |
| 1226.040 | 56.194 | −2.825 | 1.489 |

$$H_{rev}^{s}(\sigma) = H_{rev}^{s}(0) + a_3 \exp\left\{ -\left[\frac{(\sigma - b_3)}{2c_3}\right]^{2} \right\} \quad (40)$$

$$H_{for}^{f}(\sigma) = H_{for}^{f}(0) + a_4 \exp\left\{ -\left[\frac{(\sigma - b_4)}{2c_4}\right]^{2} \right\} \quad (41)$$

Another important assumption, necessary for the magnetic phenomenological description, is the reorientation process constraint based on the stress-dependent maximum strain. It can be established by considering a maximum strain as a function of the applied stress, $\varepsilon_{\max}(\sigma)$. Figure 2 presents experimental data from the works by Tickle (2000) and Kiefer and Lagoudas (2005) showing that this function can be approximated by the following equation

$$\varepsilon_{\max}(\sigma) = \begin{cases} d_1 + d_2/(1 + \exp(\sigma - \sigma_0)/d_\sigma) & \text{if } \sigma^{b} \le \sigma \le 0 \\ 0 & \textit{otherwise} \end{cases} \quad (42)$$

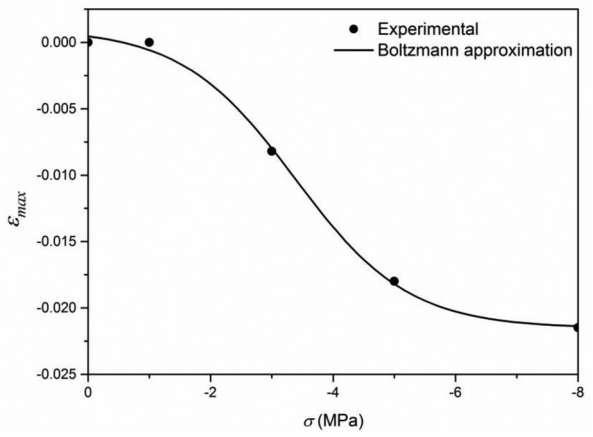


**Figure 2.** Stress dependence of the maximum induced reorientation strain.

where $d_1 = -0.0215$, $d_2 = 0.023$, $\sigma_0 = -3.376$ MPa, $d_\sigma = 0.928$ MPa, and $\sigma^b$ is the block stress defined considering that, above this stress level, all magnetic effects are suppressed. It should be pointed out that equation (42) is constructed based on experimental results during the reorientation process. Hence, this restriction can be expressed by considering the special loading condition where $\dot{H} \neq 0$.

In order to take into account differences in the phase transformation kinetics, it is possible to consider different values of the parameters $\eta_{for}^{\mathcal{M},\mathcal{A}}$ and $\eta_{rev}^{\mathcal{M},\mathcal{A}}$, adopting forward ($\dot{\varepsilon}>0$) and reverse ($\dot{\varepsilon}<0$) parameters, respectively.

## Numerical simulations

This section presents a discussion of the thermo-magneto-mechanical behavior of MSMAs predicted by the proposed model. Different behaviors are carried out considering distinct loading processes. Experimental data available in the literature are adopted as references. In brief, the idea is to test the model capability to describe phase transformations and reorientation induced by temperature, stress, or magnetic field. In this regard, thermal and stress-induced martensitic transformations, magnetic field–induced phase transformation, and magnetic field–induced martensitic variant reorientation are carried out. Experimental data from the works by Tickle (2000) and Heczko (2005) are employed as reference for the first case simulating MFIS. The second and third cases use experimental results of Karaman et al. (2006) and Karaca et al. (2007) for thermo-magneto-mechanical behavior. Numerical simulations are carried out considering different kinds of loadings to evaluate the general MSMA response. Three sections are used to split the presentation. Initially, magneto-mechanical behavior is of concern. Afterward, thermo-magneto-mechanical behavior is simulated. Finally, the general behavior is treated.

**Table 2.** Model parameters from Tickle's (2000) experimental data.

| | | | |
|---|---|---|---|
| $E^{\mathcal{A}}$(GPa) | 54 | $\eta_{for}^{\mathcal{M}}$ (Pa s) | 0.102 |
| $E^{\mathcal{M}}$(GPa) | 48 | $\eta_{rev}^{\mathcal{M}}$ (MPa s) | 0.03 |
| $\Omega^{\mathcal{A}}$(MPa/K) | 0.74 | $\eta_{for}^{\mathcal{A}}$(MPa s) | 0.1 |
| $\Omega^{\mathcal{M}}$(MPa/K) | 0.17 | $\eta_{for}^{\mathcal{A}}$(MPa s) | 0.1 |
| $\alpha_H$(MPa) | 0.0200 | $\chi^{\mathcal{M}}$ (kA/m s) | 400 |
| $\alpha$(MPa) | 85 | $\chi^{\mathcal{A}}$ (kA/m) | 0 |
| $L_0$(Pa) | 1500 | $\gamma^{\mathcal{M}}$ (kA/m s) | 500 |
| $L$(kPa) | 89 | $\gamma^{\mathcal{A}}$ (kA/m s) | 0 |
| $L_0^{\mathcal{A}}$(MPa) | 0.7 | $\delta^{\mathcal{M}}$(1/s) | 0.14 |
| $L^{\mathcal{A}}$(MPa) | 111 | $\delta^{\mathcal{A}}$(1/s) | 0 |
| $T^{\mathcal{M}}$(K) | 195 | $\mu_0(\mu\text{H m}^{-1})$ | 1.256 |

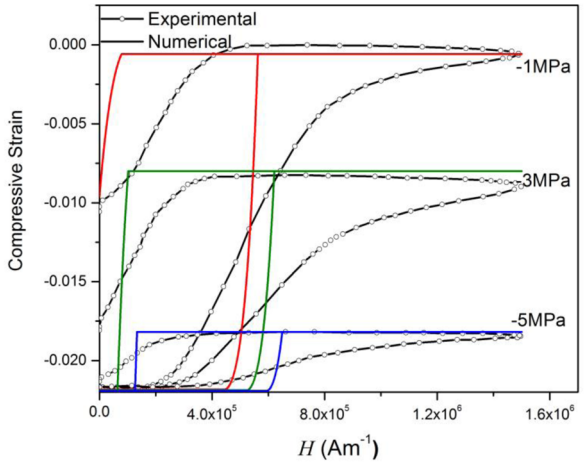


**Figure 3.** Comparison between numerical and experimental results of Tickle (2000).

### *Magneto-mechanical behavior*

This section analyzes the magnetic shape memory effect in a NiMnGa single-crystal specimen, subjected to a constant compressive stress and a variable magnetic field. Experimental results of Tickle (2000) are used as a reference considering three different stress levels. Numerical simulations are performed at $T = 183$ K employing parameters presented in Table 2.

Figure 3 presents a comparison between numerical and experimental results showing a good agreement. Note that the model is able to capture the forward phase transformation ($\mathcal{M}^- \rightarrow \mathcal{M}$) and the reverse phase transformation ($\mathcal{M} \rightarrow \mathcal{M}^-$). Moreover, the model is able to capture a residual reorientation strain upon removal of the magnetic field depending on the compressive stress value. For low stress level ($-1$ MPa), the reverse reorientation does not finish since there is not enough stress to induce the fully compressive detwinned martensite ($\mathcal{M}^-$). This effect disappears for high stress level values ($-3$ and $-5$ MPa).

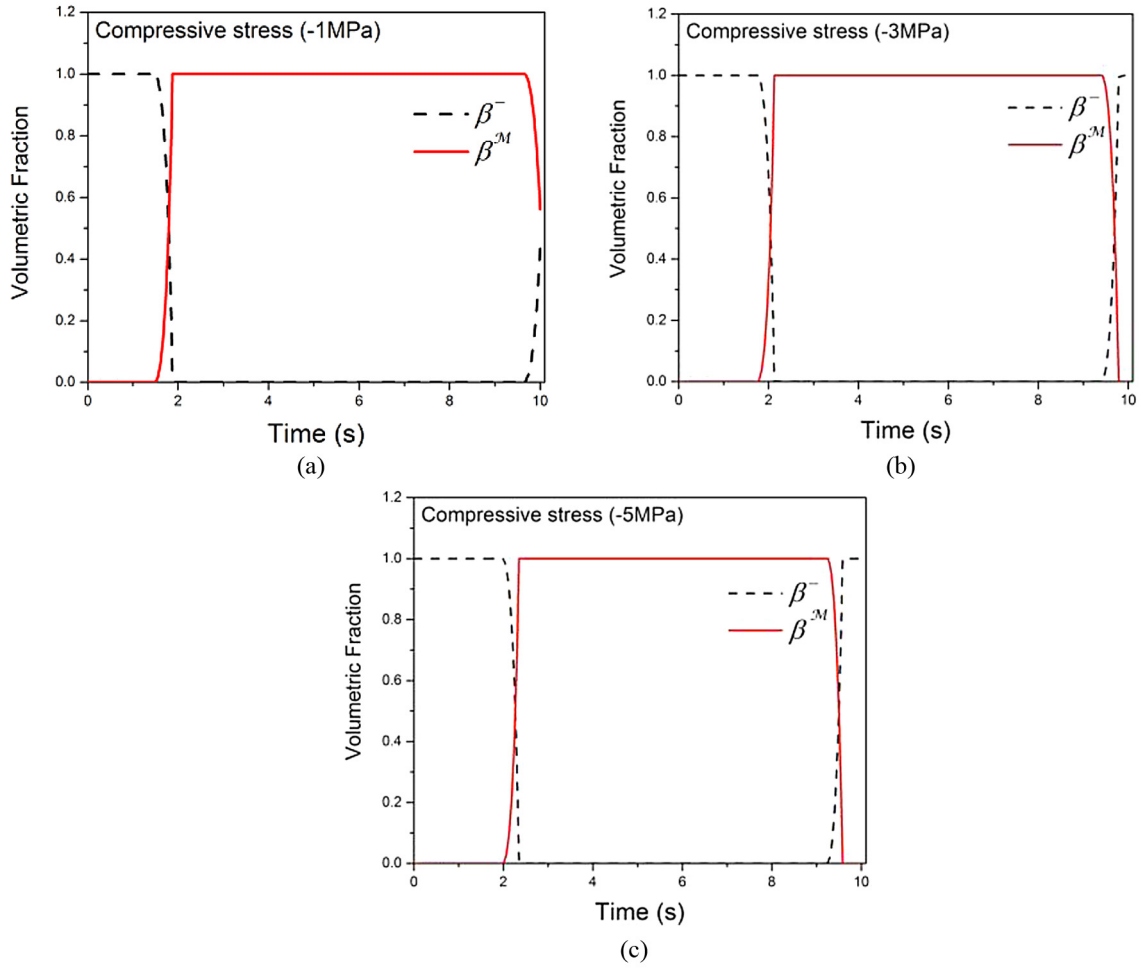


**Figure 4.** Volume fraction history for different values of compressive stress: (a) -1MPa, (b) -3MPa and (c) -5MPa.

This process can be better observed through the volume fraction time history presented in Figure 4. In general, it should be pointed out that the model captures the magneto-mechanical behavior of MSMAs and numerical simulations are in good agreement with the experimental data.

Reorientation process provides an additional mechanism to change the magnetization of the material. For stress levels below the blocking stress, the magnetic field induced changes the magnetization observed due to the fact that the magnetic easy axes in the martensitic variants have different directions with respect to a global coordinate system. In the presence of a magnetic field, the microstructural rearrangement is, therefore, always coupled to a magnetization change. Numerical simulations are performed based on experimental results of Heczko (2005) of magnetization as a function of applied magnetic field for stress level of −1.0 MPa. Model parameters are presented in Table 3.

Figure 5(a) shows a comparison between numerical and experimental results of the martensitic magnetization as a function of applied magnetic field for stress level of −1.0 MPa. Initially, MSMA sample is exposed to compressive mechanical loading, which produces compression-induced reorientation of martensite ($\beta^-$). Once the critical field for variant reorientation has been

**Table 3.** Model parameters from Heczko's (2005) experimental data.

| | | | |
|---|---|---|---|
| $E^{\mathcal{A}}$(GPa) | 54 | $\eta^{\mathcal{M}}_{for}$ (Pa s) | 0.102 |
| $E^{\mathcal{M}}$(GPa) | 48 | $\eta^{\mathcal{M}}_{rev}$ (MPa s) | 0.03 |
| $\Omega^{\mathcal{A}}$(MPa/K) | 0.74 | $\eta^{\mathcal{A}}_{for}$(MPa s) | 0.1 |
| $\Omega^{\mathcal{M}}$(MPa/K) | 0.17 | $\eta^{\mathcal{A}}_{for}$(MPa s) | 0.1 |
| $\alpha_H$(MPa) | 0.0200 | $\chi^{\mathcal{M}}$ (kA/m s) | 185 |
| $\alpha$(MPa) | 85 | $\chi^{\mathcal{A}}$ (kA/m) | 0 |
| $L_0$(Pa) | 1500 | $\gamma^{\mathcal{M}}$ (kA/m s) | 288 |
| $L$(kPa) | 89 | $\gamma^{\mathcal{A}}$ (kA/m s) | 0 |
| $L_0^{\mathcal{A}}$(MPa) | 0.7 | $\delta^{\mathcal{M}}$ (1/s) | 0.485 |
| $L^{\mathcal{A}}$(MPa) | 111 | $\delta^{\mathcal{A}}$ (1/s) | 0 |
| $T^{\mathcal{M}}$(K) | 195 | $\mu_0(\mu\mathrm{H\,m^{-1}})$ | 1.256 |
| $H^s_{for}(0)$ (kA/m) | 211.981 | $H^f_{for}(0)$ (kA/m) | 540.0 |
| $H^s_{ref}(0)$ (kA/m) | 342.163 | $H^f_{ref}(0)$ (kA/m) | −4.605 |

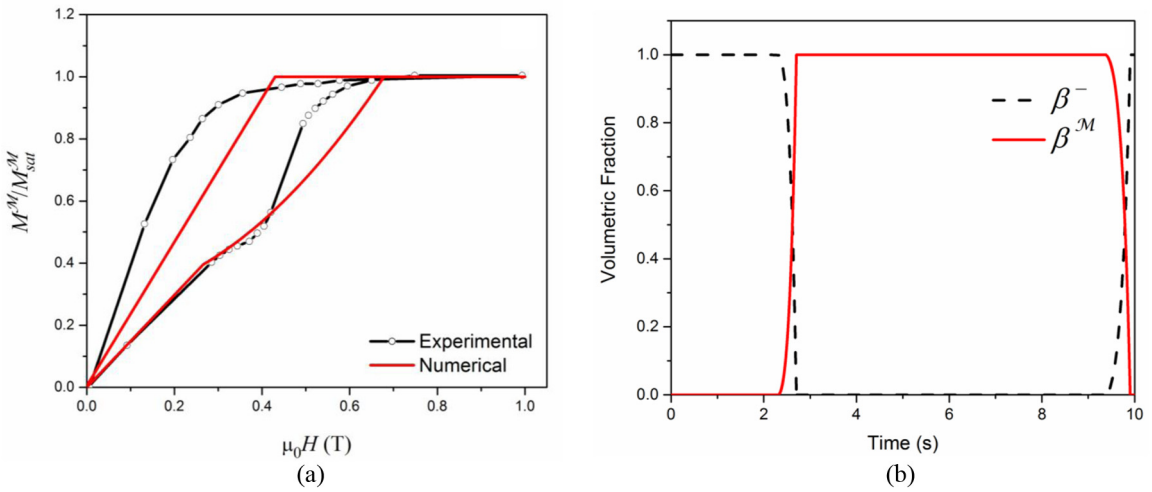


**Figure 5.** (a) Comparison between numerical and experimental results of Heczko (2005) of the martensitic magnetization as a function of applied magnetic field for stress level of $-1.0$ MPa and saturation magnetization $M^{\mathcal{M}}_{sat} = 622\times10^3$ H m$^{-1}$ and (b) volume fraction time history.

**Table 4.** Model parameters based on Karaman et al.'s (2006) experimental data.

| | | | |
|---|---|---|---|
| $E^{\mathcal{A}}$(GPa) | 6 | $\eta^{\mathcal{M}}_{for}$ (MPa s) | 0.102 |
| $E^{\mathcal{M}}$(GPa) | 12.5 | $\eta^{\mathcal{M}}_{rev}$ (MPa s) | 0.102 |
| $\Omega^{\mathcal{A}}$(MPa/K) | 0.74 | $\eta^{\mathcal{A}}_{for}$(MPa s) | 0.1 |
| $\Omega^{\mathcal{M}}$(MPa/K) | 0.17 | $\eta^{\mathcal{A}}_{for}$(MPa s) | 0.1 |
| $\alpha_H$(MPa) | 0.0245 | $\chi^{\mathcal{M}}$ (kA/m s) | 500 |
| $\alpha$(MPa) | 174 | $\chi^{\mathcal{A}}$ (kA/m) | 250 |
| $L_0$(MPa) | 0.81 | $\gamma^{\mathcal{M}}$ (kA/m s) | 500 |
| $L$(MPa) | 89 | $\gamma^{\mathcal{A}}$ (kA/m s) | 250 |
| $L^{\mathcal{A}}_0$(MPa) | 0.7 | $\delta^{\mathcal{M}}$ (1/s) | 0.45 |
| $L^{\mathcal{A}}$(MPa) | 0.7 | $\delta^{\mathcal{A}}$ (1/s) | 0.225 |
| $T^{\mathcal{M}}$(K) | 195 | $\mu_0(\mu$H m$^{-1})$ | 1.256 |

reached, the magnetic field–favored variant ($\mathcal{M}$) nucleates and a sharp change in the slope of the magnetization curve occurs. This can be observed through the volume fraction time history presented in Figure 5(b). At high fields, the stress-favored variant is completely eliminated and the material is magnetically saturated in the field direction, resulting in a single-variant domain. The reverse reorientation follows the same idea. Note that further decrease in the magnetic field completely eliminates variant ($\mathcal{M}$) at the threshold value of $H^f_{rev}$ and for the resulting single compressive detwinned martensite variant ($\mathcal{M}^-$).

### *Thermo-magneto-mechanical behavior*

Thermo-magneto-mechanical behavior of MSMAs is now of concern considering different loading processes. Initially, pseudoelastic and shape memory effects are of concern using experimental results obtained by Karaman et al. (2006) for compressive tests at four different temperatures: 193, 213, 223, and 233 K. Parameter adjustment is performed in order to match experimental data at $T = 193$ K being presented in Table 4.

Figure 6 shows the comparison between numerical and experimental results. Loading process considers a mechanical loading from zero to a maximum value and then an unloading back to zero. All tests are performed with stress driving case with constant temperature and null magnetic field. Results show that temperature increase promotes a vertical shift of the hysteresis loop promoting a change from shape memory (for temperatures below $T^{\mathcal{M}}$—Figure 6(a)) to pseudoelastic effect (for temperatures above $T^{\mathcal{M}}$—Figure 6(b) to (d)). The model is able to capture all kinds of behaviors, at different temperatures, presenting a residual strain for low temperature (Figure 6(a)). Figure 7 shows volume fraction evolution for each one of the numerical tests, being coherent with the stress–strain curves. It should be highlighted that numerical results are in close agreement with experimental data.

The influence of magnetic field is now of concern by considering experimental data of Karaca et al. (2007) as a reference. These experimental tests treat compressive tests on Ni-Mn-Ga wires subjected to different, constant, non-zero magnetic field and a constant temperature. Figure 8(a) shows the experimental pseudoelastic response at $T = 213$ K under zero (black line) and 620 kA m$^{-1}$ applied magnetic field (red line), where the difference between the plateau stress levels with and without magnetic field is defined as magnetostress ($\sigma_{mag}$). Prior to each stress cycle, the external magnetic field is applied along the [011] direction, perpendicular to the loading direction, and kept constant during the loading.

Numerical simulations are carried out based on these experimental tests with parameters presented in Table 4. Figure 8(b) shows numerical simulations and

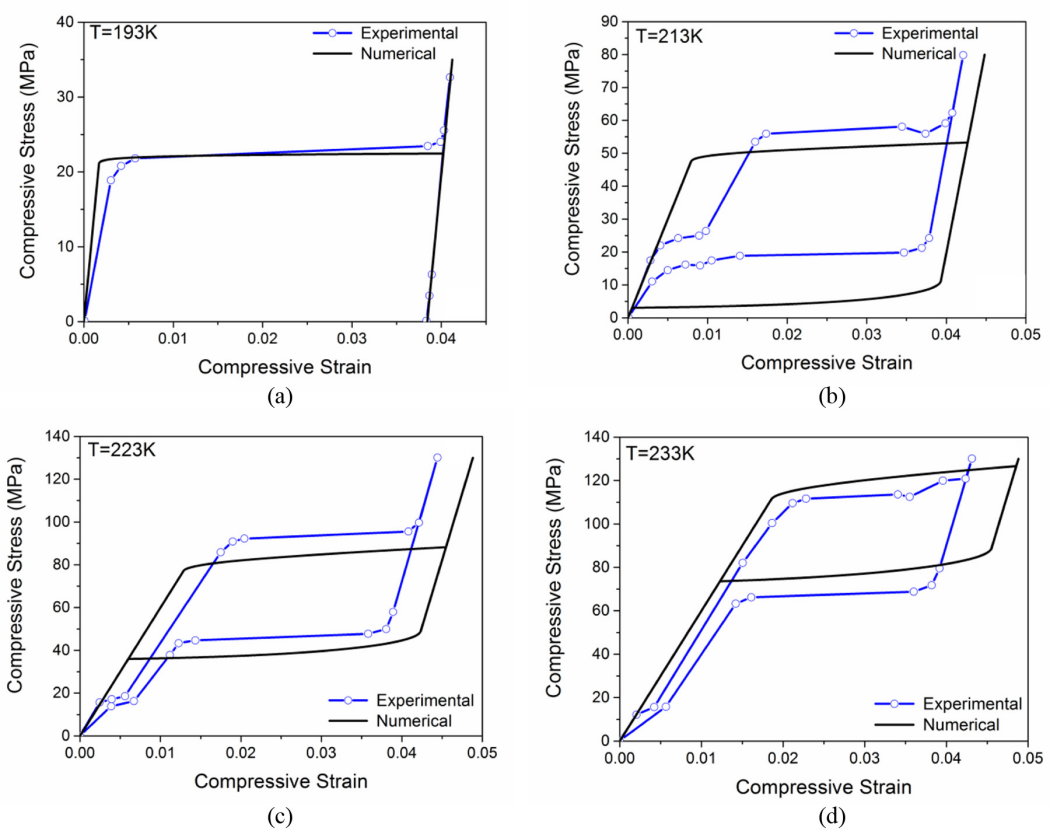


**Figure 6.** Comparison between numerical and experimental results of Karaman et al. (2006): (a) T=193K, (b) T=213K, (c) 223K and (d) T=233 K.

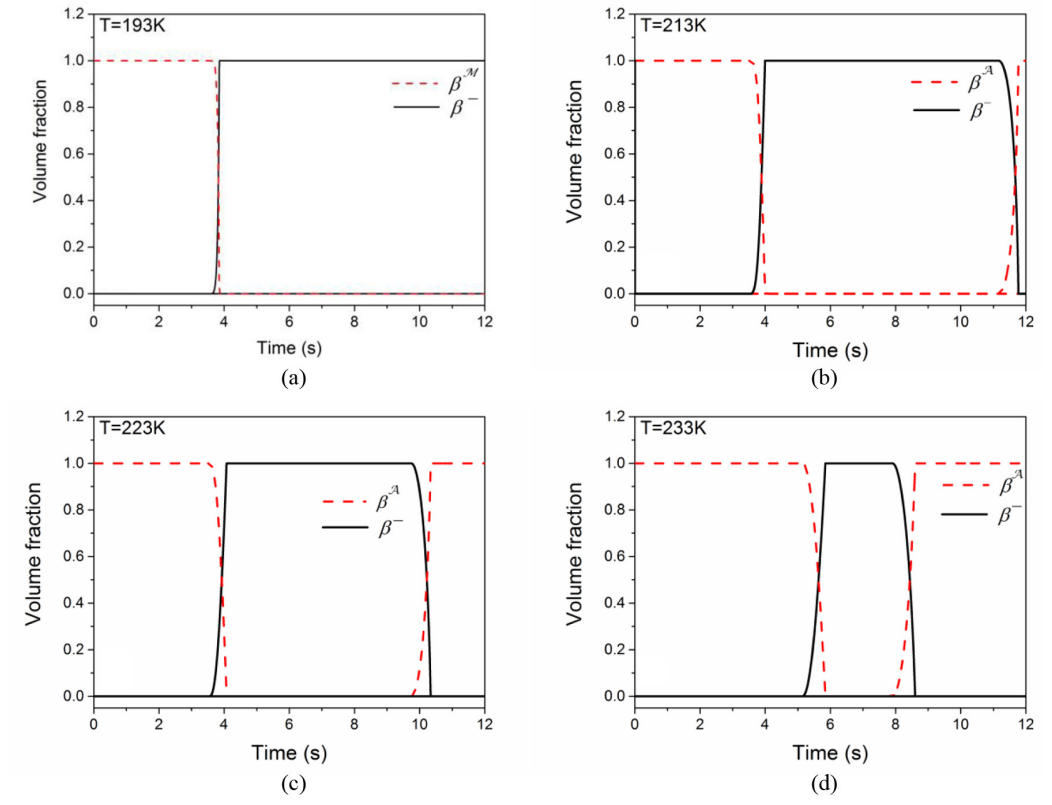


**Figure 7.** Volume fraction time history at different temperatures: (a) T=193K, (b) T=213K, (c) 223K and (d) T=233 K.

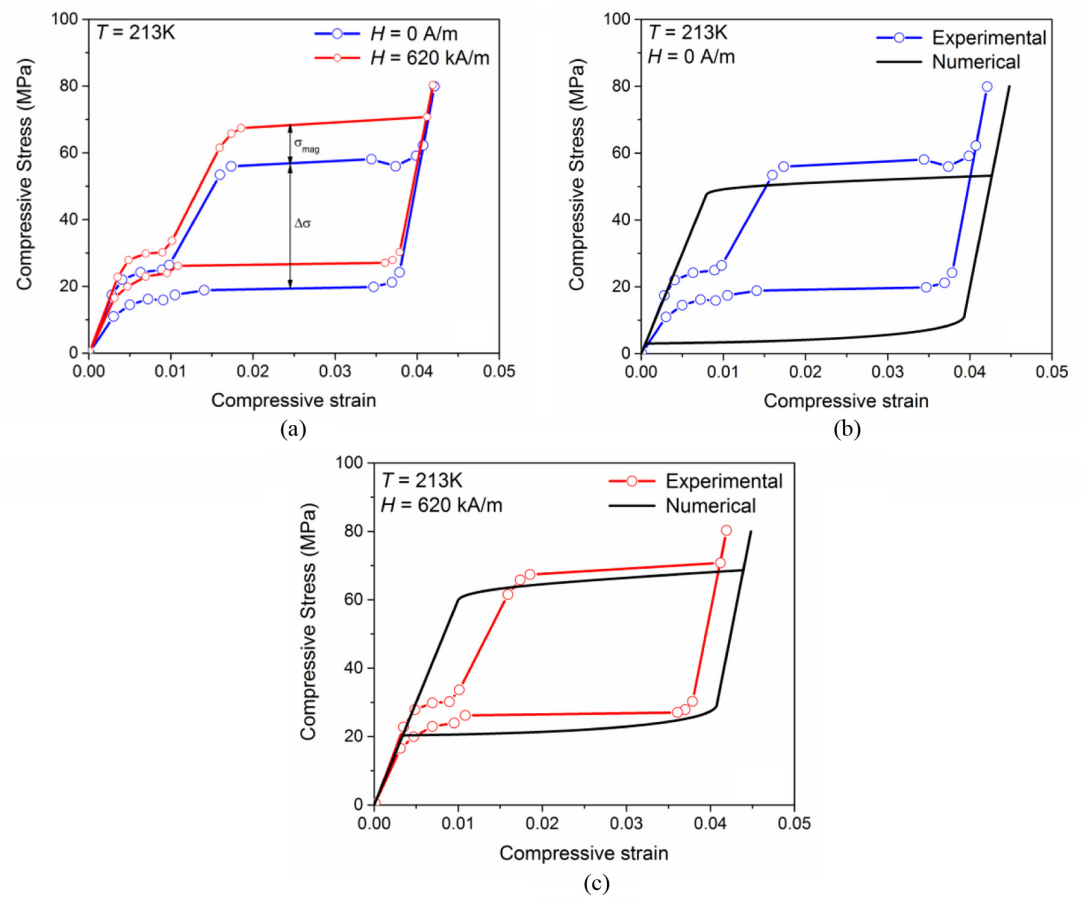


**Figure 8.** Stress–strain curves subjected to different magnetic fields: (a) experimental stress–strain curves (Karaca et al., 2007), (b) comparison between numerical and experimental results with $H = 0\,\mathrm{kA\,m^{-1}}$, and (c) comparison between numerical and experimental results with $H = 620\,\mathrm{kA\,m^{-1}}$.

experimental data for $T = 213$ K subjected to a null magnetic field. Figure 8(c) presents the same case but considering a magnetic field ($H = 620\,\mathrm{kA\,m^{-1}}$). Once again, it is possible to observe that the model is able to capture the thermomechanical behavior of the MSMA.

## General behavior

At this moment, it is possible to say that the proposed model is able to capture the general thermo-magneto-mechanical behavior of MSMAs, which is attested by several experimental tests. Hence, some numerical simulations are presented in order to show more details about the MSMAs behavior. This is done considering material properties presented in Table 4.

Shape memory effect is related to the shape recovery capacity being associated with phase transformation that eliminates residual strain caused by previous mechanical loading. In this regard, loading process presented in Figure 6(a) can be used to explain the phenomenon. Both temperature and magnetic field can be employed to promote this phase transformation, promoting the specimen recover. The mechanical and thermal loadings employed are shown in Figure 9. Initially, MSMA sample is exposed to compression mechanical loading which leads to compression-induced reorientation of martensite ($\beta^-$). After that, the material is unloaded to zero stress, and the thermal

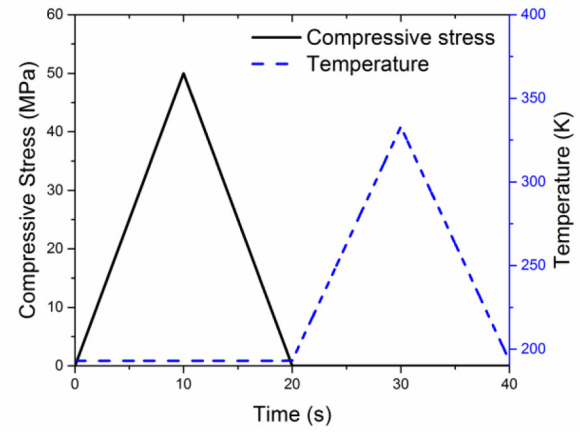


**Figure 9.** Mechanical and thermal loading process.

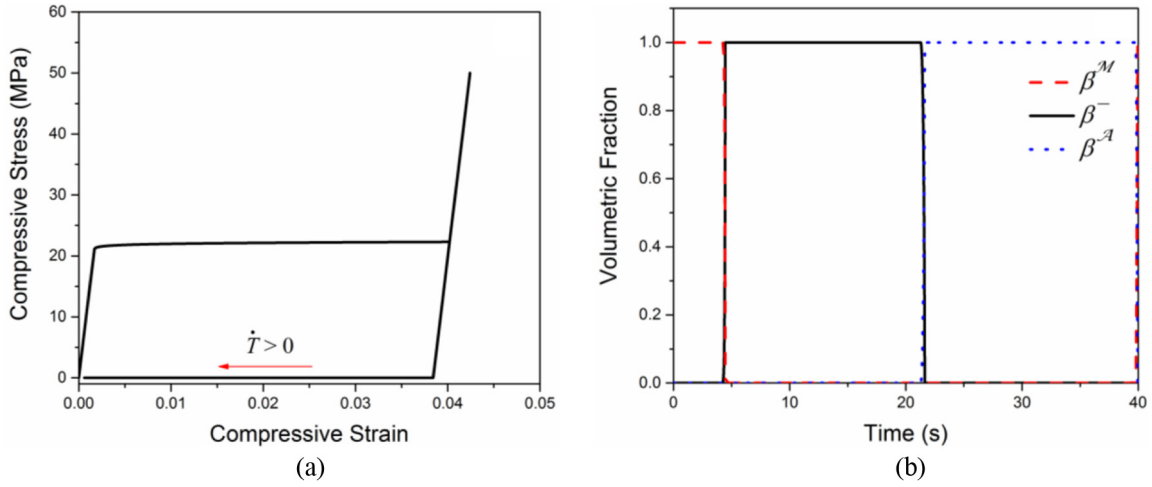


**Figure 10.** Shape memory effect induced by temperature: (a) stress–strain–temperature curve and (b) volume fraction time history.

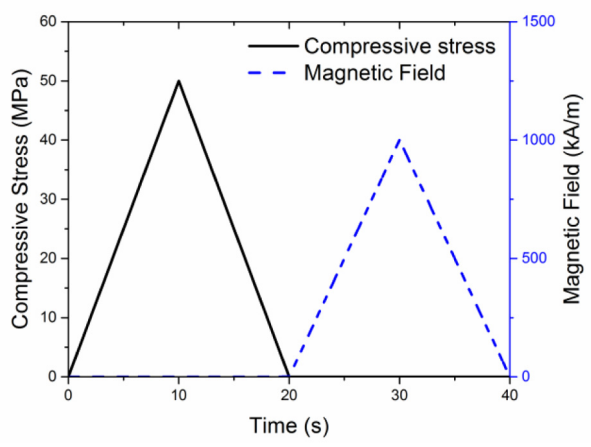


**Figure 11.** Mechanical and magnetic loading process.

loading is incrementally applied inducing the phase transformation to austenite ($\mathcal{A}$). The reverse transformation induced by heating the sample in a stress-free state can fully recover the martensitic phase ($\beta^{\mathcal{M}}$). Figure 10 presents the stress–strain–temperature curve together with volume fraction evolutions, showing recovery of the sample. Note that after the mechanical loading, residual strain is eliminated. Similar behavior can be achieved exposing the MSMA sample to a magnetic field at zero stress. The mechanical and magnetic loadings employed are shown in Figure 11. The detwinned martensite, induced by compression ($\beta^{-}$), is converted to a new martensitic variant ($\beta^{\mathcal{M}}$). Figure 12 presents the stress–strain–magnetic field and volume fraction evolutions, showing recovery of the same sample. Note that for magnetic loading, reorientation process is the essential driving aspect for shape recovery. On the other hand, the phase transformation is the essential driving during temperature loading.

This behavior makes MSMAs a flexible smart material that can combine thermo-magneto-mechanical behavior for different purposes. It should be highlighted that hysteretic temperature and magnetic field dependence are interesting to be exploited in different situations. In order to highlight this general behavior, Figure 13 shows the stress–strain curves for different values of constant applied magnetic field assuming temperature of 195 K (left panel) and for different values of temperature vanishing magnetic field (right panel). When magnetic field vanishes, the residual strain remains when the compressive stress is removed. The residual strain decreases when the applied field increases changing the increase in the critical stress level where field-preferred variant reorientation begins to occur. The same behavior is observed for increasing the temperature where phase transformation is explored.

## Conclusion

A macroscopic constitutive theory is developed to describe the thermo-magneto-mechanical behavior of MSMAs. This novel model is based on the previous contribution of Paiva et al. (2005) and Oliveira et al. (2016) for classic SMAs. The new model incorporates magnetic effects being able to describe the magnetic field–induced phase transformation and magnetic field–induced martensitic variant reorientation under different loading conditions. Numerical simulations are carried out, being compared with experimental data available in the literature. Results show different features associated with combinations of thermo-magneto-mechanical loadings. As a conclusion, the model captures the general thermo-magneto-mechanical

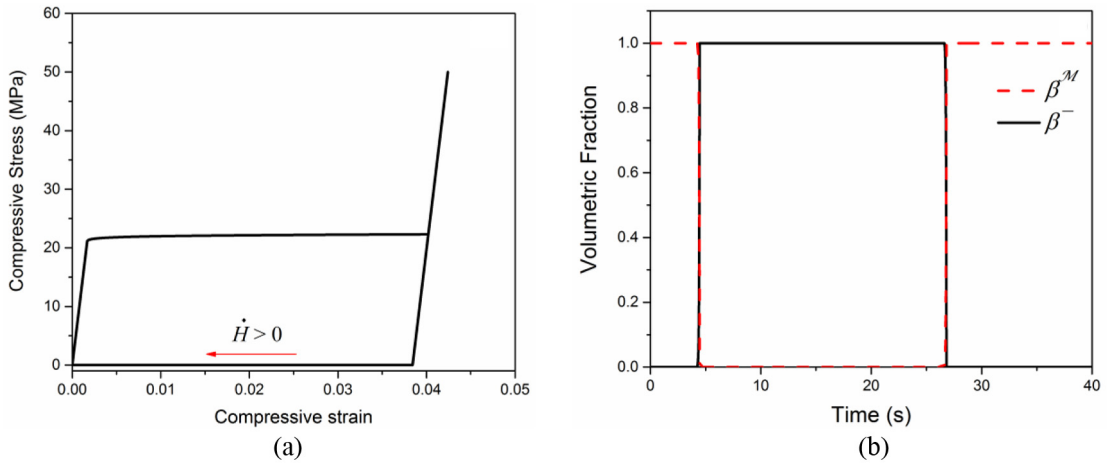


**Figure 12.** Shape memory effect induced by magnetic field: (a) stress–strain–magnetic field curve and (b) volume fraction time history.

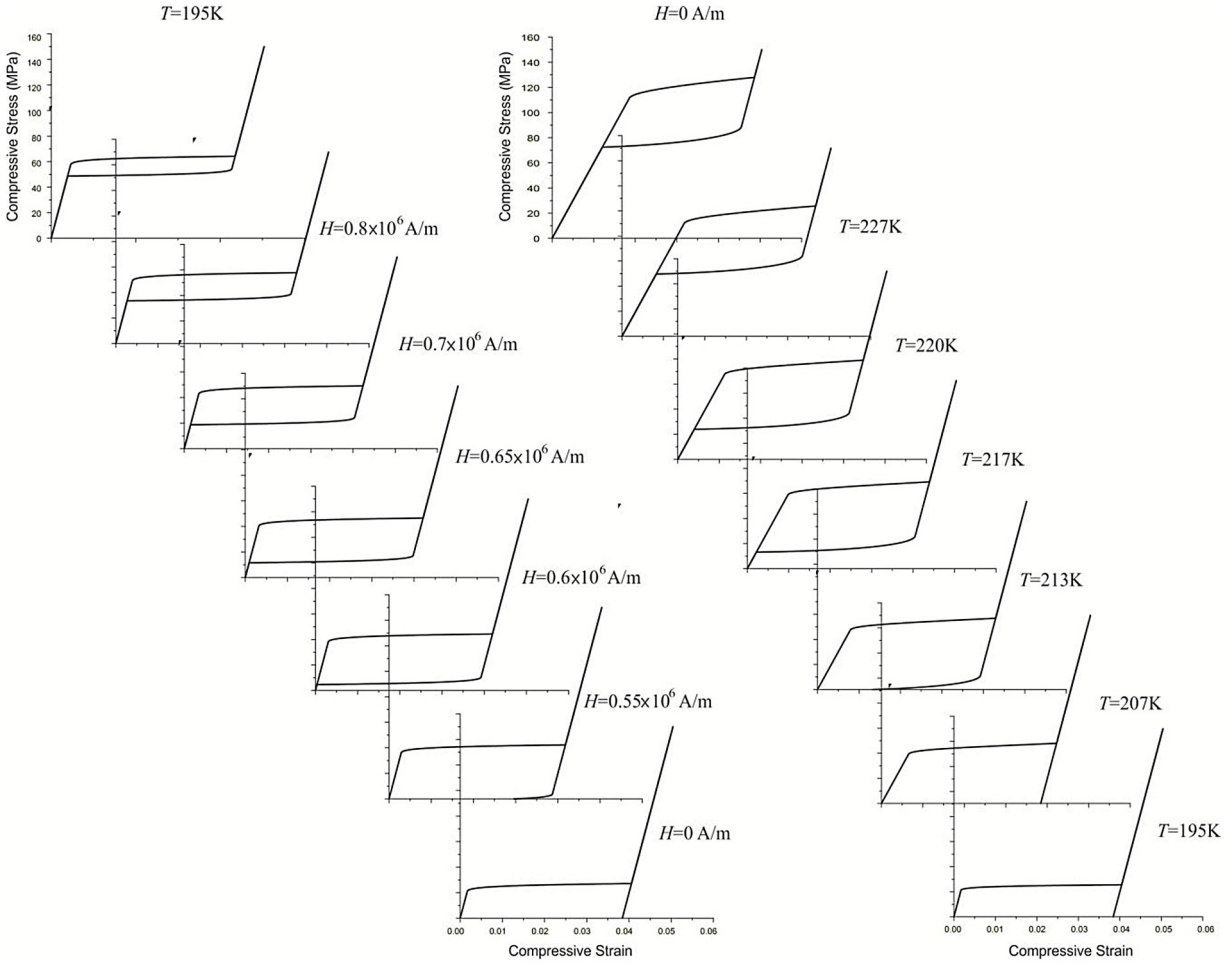


**Figure 13.** Stress–strain curves with different values of constant applied magnetic field assuming temperature of 195 K (left panel) and stress–strain curves with different values of temperature with vanished magnetic field (right panel).

behavior of MSMAs, being able to describe several phenomena in a flexible way.

## Declaration of conflicting interests

The author(s) declared no potential conflicts of interest with respect to the research, authorship, and/or publication of this article.

## Funding

The author(s) disclosed receipt of the following financial support for the research, authorship, and/or publication of this article: This work is supported by the Brazilian Research Agencies CNPq, CAPES, and FAPERJ and by The Air Force Office of Scientific Research (AFOSR).

## ORCID iD

Marcelo A Savi https://orcid.org/0000-0001-5454-5995

## References

Brinson LC (1993) One-dimensional constitutive behavior of shape memory alloys: thermomechanical derivation with non-constant material functions and redefined martensite internal variable. *Journal of Intelligent Material Systems and Structures* 4: 229–242.

Bruno NM, Wang S, Karaman I, et al. (2017) Reversible martensitic transformation under low magnetic fields in magnetic shape memory alloys. *Scientific Reports* 7: 40434–40444.

Chernenko VA, Mullner P and Kostorz G (2004) A microscopic approach to the magnetic-field-induced deformation of martensite (magnetoplasticity). *Journal of Magnetism and Magnetic Materials* 267: 325–334.

Couch RN, Sirohi YJ and Chopra I (2007) Development of a quasi-static model of NiMnGa magnetic shape memory alloy. *Journal of Intelligent Material Systems and Structures* 18: 611–622.

Guo Z, Li H, Wan Q, et al. (2014) A model to describe the magnetomechanical behavior of martensite in magnetic shape memory alloy. *Advances in Condensed Matter Physics* 2014: 295436.

Haldar K, Lagoudas DC and Karaman I (2014) Magnetic field-induced martensitic phase transformation in magnetic shape memory alloys: modeling and experiments. *Journal of the Mechanics and Physics of Solids* 69: 33–66.

Heczko O (2005) Magnetic shape memory effect and magnetization reversal. *Journal of Magnetism and Magnetic Materials* 290–291: 787–794.

Henry CP, Bono D, Feuchtwanger J, et al. (2002) AC field-induced actuation of single crystal Ni-Mn-Ga. *Journal of Applied Physics* 91: 7810–7811.

Hirsinger L and Lexcellent C (2003) Modelling detwinning of martensite platelets under magnetic and (or) stress actions on Ni-Mn-Ga alloys. *Journal of Magnetism and Magnetic Materials* 254–255: 275–277.

James RD and Wuttig M (1998) Magnetostriction of martensite. *Philosophical Magazine A* 77(5): 1273–1299.

Jin YM (2009) Domain microstructure evolution in magnetic shape memory alloys: phase-field model and simulation. *Acta Materialia* 57: 2488–2495.

Kainuma R, Imano Y, Ito W, et al. (2006) Magnetic-field-induced shape recovery by reverse phase transformation. *Nature* 439: 957–960.

Karaca HE, Karaman I, Basaran B, et al. (2007) On the stress-assisted magnetic-field-induced phase transformation in $Ni_2MnGa$ ferromagnetic shape memory alloys. *Acta Materialia* 55: 4253–4269.

Karaca HE, Karaman I, Basaran B, et al. (2009) Magnetic field-induced phase transformation in NiMnCoIn magnetic shape-memory alloys—a new actuation mechanism with large work output. *Advanced Functional Materials* 19: 983–998.

Karaca HE, Karaman I, Lagoudas DC, et al. (2003) Recoverable stress-induced martensitic transformation in a ferromagnetic CoNiAl alloy. *Scripta Materialia* 49: 831–836.

Karaman I, Karaca HE, Basaran B, et al. (2006) Stress-assisted reversible magnetic field-induced phase transformation in $Ni_2MnGa$ magnetic shape memory alloys. *Scripta Materialia* 55(4): 403–406.

Kiefer B and Lagoudas DC (2005) Magnetic field-induced martensitic variant reorientation in magnetic shape memory alloys. *Philosophical Magazine* 85(33–35): 4289–4329.

Kiefer B and Lagoudas DC (2008) Modeling of the variant reorientation in magnetic shape-memory alloys under complex magnetomechanical loading. *Materials Science and Engineering: A* 481–482: 339–342.

Kiefer B and Lagoudas DC (2009) Modeling the coupled strain and magnetization response of magnetic shape memory alloys under magnetomechanical loading. *Journal of Intelligent Material and Systems and Structures* 20: 143–170.

Kiefer B, Karaca HE, Lagoudas DC, et al. (2007) Characterization and modeling of the magnetic field-induced strain and work output in $Ni_2MnGa$ magnetic shape memory alloys. *Journal of Magnetism and Magnetic Materials* 312: 164–175.

Lemaitre J and Chaboche JL (1990) *Mechanics of Solid Materials*. London: Cambridge University Press.

Li LJ, Lei CH, Shu YC, et al. (2011) Phase-field simulation of magnetoelastic couplings in ferromagnetic shape memory alloys. *Acta Materialia* 59: 2648–2655.

Liang Y, Sutou Y, Wada T, et al. (2003) Magnetic field-induced reversible actuation using ferromagnetic shape memory alloys. *Scripta Materialia* 48: 1415–1419.

Liu J, Gottschall T, Skokov KP, et al. (2012) Giant magnetocaloric effect driven by structural transitions. *Nature Materials* 11(7): 620–626.

Marioni MA, O'Handley RC, Allen SM, et al. (2005) The ferromagnetic shape-memory effect in Ni-Mn-Ga. *Journal of Magnetism and Magnetic Materials* 290: 35–41.

Müllner P, Chernenko VA and Kostorz G (2002) A microscopic approach to the magnetic-field-induced deformation of martensite (magnetoplasticity). *Journal of Magnetism and Magnetic Materials* 267: 325–334.

Murray SJ, Marioni M, Allen SM, et al. (2000) 6% magnetic-field-induced strain by twin-boundary motion in ferromagnetic Ni-Mn-Ga. *Applied Physics Letters* 77(6): 886–888.

Oliveira SA, Savi MA and Zouain N (2016) A three-dimensional description of shape memory alloy thermomechanical behavior including plasticity. *Journal of the Brazilian Society of Mechanical Sciences and Engineering* 38(5): 1451–1472.

Paiva A, Savi MA and Braga AMB (2005) A constitutive model for shape memory alloys considering tensile—compressive asymmetry and plasticity. *International Journal of Solids and Structures* 42: 3439–3457.

Penga Q, Huanga J, Chena M, et al. (2017) Phase-field simulation of magnetic hysteresis and mechanically induced remanent magnetization rotation in Ni-Mn-Ga ferromagnetic shape memory alloy. *Scripta Materialia* 127: 49–53.

Rockafellar RT (1970) *Convex Analysis*. Princeton, NJ: Princeton University Press.

Tanaka K (1986) A thermomechanical sketch of shape memory effect: one-dimensional tensile behavior. *Research Mechanical* 1: 251–263.

Tickle R (2000) *Ferromagnetic shape memory materials*. PhD Thesis, University of Minnesota, Minneapolis, MN.

Tickle R and James RD (1999) Magnetic and magnetomechanical properties of $Ni_2MnGa$. *Journal of Magnetism and Magnetic Materials* 195(3): 627–638.

Ullakko K, Huang JK, Kantner C, et al. (1996) Large magnetic-field-induced strains in $Ni_2MnGa$ single crystals. *Applied Physics Letters* 69(13): 1966–1968.